Shallow sampling by multi-shot laser ablation and its application within U-Pb zircon geochronology

Eoghan P. Corbett[a,b,*], Antonio Simonetti[a], Phil Shaw[c], Loretta Corcoran[a], Quentin G. Crowley[b], Brendan C. Hoare[b]

[a] *Department of Civil and Environmental Engineering and Earth Sciences (CEEES), University of Notre Dame, IN 46556, USA*
[b] *Department of Geology, Trinity College Dublin, Dublin 2, Ireland*
[c] *Nu Instruments Ametek, Wrexham LL13 9XS, Wales, UK*

A B S T R A C T

The interaction of incident laser radiation and sample substrate is complex and difficult to predict. Natural zircons are often both structurally and chemically heterogeneous in 3-dimensional space. Encountering growth-related, structural micro-heterogeneities, inclusions and chemical complexities is almost inevitable during a static ablation of several tens of seconds. A multi-shot approach to laser ablation described here implements a minimal sample exposure time to incident laser radiation by applying multiple 1 Hz shots to a single sample location in delayed succession. This process can be conceptualised as a "slowing down" of a high-frequency (5–20 Hz) static laser ablation inductively coupled plasma mass spectrometry (LA-ICP-MS) analysis until each laser pulse is distinct albeit transient. The ability to integrate and collate signal pulses for a small number of consecutive laser shots, as opposed to continuously pulsing the laser, produces precise age determinations (~1% reproducibility, 2σ level) on small sample volumes (704 $\pm$ 23 μm^3 on 91500 zircon standard). The multi-shot LA-ICP-MS protocol employed here significantly reduces the effect of 'downhole' fractionation as the resultant craters are extremely shallow (as shallow as 0.56 $\pm$ 0.02 μm on 91500 zircon standard) and maintain an aspect ratio of ≪1. Further benefits include a reduced probability of thermally induced effects (e.g., substrate melting), plasma loading, and the potential for signal mixing (with depth) in a heterogeneous sample.

1. Introduction

Zircon U-Pb ages determined by the benchmark isotope dilution thermal ionization mass spectrometry (ID-TIMS) method, are often systematically at variance (1–2%, 2σ) to those determined by in-situ laser ablation-inductively coupled plasma mass spectrometry (LA-ICP-MS) for the same sample set (Horstwood et al., 2016; Košler et al., 2013). Despite rapid advances in LA-ICP-MS instrumentation, techniques, pre-treatments and a converging consensus on how zircon U-Pb data-reduction protocols are to be employed (e.g., Horstwood et al., 2016), laser induced elemental fractionation (LIEF) arguably still remains the single greatest obstacle in achieving the analytical precision and accuracy associated with other, often more costly in-situ techniques (e.g., secondary ion mass spectrometry, SIMS; Chew et al., 2018)

Non-stoichiometric sampling of the target analyte due to LIEF has often been reported for high-frequency, static ablation protocols used extensively in U-Pb geochronological studies (e.g., Fryer et al., 1995; Hirata and Nesbitt, 1995; Longerich et al., 1996; Horn et al., 2000;

Kuhn et al., 2004). Laser operational parameters directly affect the properties of laser-generated aerosols, particle-size distribution, dehydration, atomization and ionization efficiency, and hence directly influence the degree of fractionation occurring within the system (Bleiner and Günther, 2001; Guillong and Günther, 2002; Koch et al., 2002; Horn and Günther, 2003; Kuhn et al., 2004).

Various studies demonstrate a minimisation of LIEF by utilizing a short (157 or 193 nm) laser wavelength (e.g., Russo et al., 2000; Jackson et al., 2004; Kroslakova and Günther, 2007), maintaining focus above the material surface (Marillo-Sialer et al., 2014; Liu et al., 2000), careful adjustment of carrier gas flow and composition (Günther and Heinrich, 1999; Horn and Günther, 2003; Kroslakova and Günther, 2007), and avoiding melting or particle re-deposition over the sample surface by utilizing shorter pulse widths (Eggins et al., 1998; Fernández et al., 2007; Shaheen et al., 2012). The most practicable means by which LIEF can be minimised however, is by ensuring craters are of a critical aspect ratio (depth/diameter) < 1 (Mank and Mason, 1999, 2001).

* Corresponding author at: Department of Geology, Trinity College Dublin, Dublin 2, Ireland.
E-mail address: corbetep@tcd.ie (E.P. Corbett).

For zircon, a high affinity of U (and Hf) for Zr results in its retention within the crater during a laser induced phase transition of SiO_2 to ZrO_2 (Kuhn et al., 2009). Both Si and Pb show no such affinity and freely are mobilised out of ablation craters as condensate independently of their diameter (Košler et al., 2005, Kuhn et al., 2009). U retention during ablation was shown by Kuhn et al. (2009) to be crater-size dependent. Where an aspect ratio can be kept $\ll 1$, LIEF of this kind can be reduced well within the associated analytical uncertainty, eliminating the need to propagate any additional uncertainty (Horstwood, 2008).

Authors of similar, previous work to that presented here (e.g., Cottle et al., 2009, 2012) demonstrated the utility and potential of a single-shot approach to laser ablation for minimising sample destruction and improving depth resolution, by integrating discrete peaks generated by consecutive single laser pulses. The analytical procedure presented in this contribution differs from these previous works insofar as shot-to-shot resolution is not the primary concern. A complete and ultra-fast washout of the analyte (and the associated small-volume ablation cell) is consequently not required. Instead, the relatively large volume of the standard ablation cell (~ 8 cm^3) is utilised in concert with a short washout duration (3 s) to maintain an elevated signal throughout an analysis, with only a partial washout between laser pulses. Hence fewer shots need be applied to the sample surface, as isotope ratio determination can be made for each 1 Hz laser shot. Herein lies the advantage of a multi-shot approach to laser ablation; the resulting depth achieved after either 30 or 10 shots is much shallower than a conventional laser analysis (e.g., up to 96.5% shallower than some other ablation protocols (Horstwood, 2008), and demonstrably minimises U-Pb 'downhole' fractionation. The approach to laser ablation analysis described here may help to overcome other sources of laser induced elemental fractionation (LIEF) such as, thermally induced effects (e.g., substrate melting), plasma loading effects and crucially, intra-crystalline signal mixing (with depth).

The analytical protocol reported here routinely produces weighted mean age determinations largely reproducible to $\leq 1\%$ (2σ) on small sample volumes (as low as 704 ± 23 µm^3) with a 40 µm diameter spot, demonstrating an overall improvement in internal precision over that of a single-shot approach alone (Cottle et al., 2009). The multi-shot method outlined here is validated with results obtained on zircon standard reference materials and samples dated using benchmark ID-TIMS.

2. Materials and methods

2.1. Instrumentation

Ablations were performed using a UP-213 frequency quintupled deep UV ($\lambda = 213$ nm) solid-state Nd:YAG laser ablation sampling system (New Wave Research, USA). This was coupled to a Nu Attom High Resolution (HR)-ICP-MS instrument (Nu Instruments, UK), at the Midwest Isotope and Trace Element Research Analytical Center (MITERAC), University of Notre Dame, USA. Analytical set-up and operating parameters are summarised in Table 1. The sweep gas flow rates and temperatures within spray chamber and desolvating membrane were monitored and maintained with a Aridus II Desolvating Nebulising system (CETAC Technologies, USA). The sweep gas flow rate proved particularly influential in the resultant reproducibility of U/Pb ratios, given the small volumes of analyte being sampled. Ideal laser and sweep gas set-up and parameters were 'dialled in' over the course of multiple analytical sessions by monitoring reproducibility on measured U/Pb ratios of NIST612 standard glass.

The Nu Attom HR-ICP-MS instrument was operated in low resolution, peak jump detector mode during a time-resolved analysis (TRA). In this mode, the magnet position is static or 'parked' at a mass of interest (i.e., 206) in the middle of the Pb-isotope range. The deflector plate voltages can therefore achieve very fast and reliable scanning or peak jumping over the narrow mass range set by the operator, in this

instance between masses 202 and 238. The *fastscan ion optics* facility of the Nu Attom allows for a maximal acquisition time at the top of each mass peak defined by the user in the TRA analysis file during a sweep. The TRA used herein to derive ages operated at differing sweep and cycle settings depending on the shot count used. Dwell times were fixed at 500 µs on each mass of interest, namely; 202, 204, 206, 207, 208, 235 and 238. Magnet calibration and detector tuning were conducted prior to TRA by aspirating a tune solution containing 0.5 ppb U and Pb in dry plasma mode. A subsequent, secondary check of the tune conditions was carried out in-situ on NIST612 standard glass by laser ablation after He was introduced into the system (1 Lmin^{-1}). The working values used for NIST612 are from Woodhead and Hergt (2001).

Crater depth determinations and imaging were made using a Profilm3D (Filmetrics, USA) White Light Interferometer (WLI) and a TESCAN TIGER MIRA3 variable pressure field-emission scanning electron microscope (FE-SEM) equipped with a secondary electron detector at the iCRAG lab, Trinity College Dublin, respectively. The WLI technique optically measures surface roughness and texture, allowing a three-dimensional visualization and quantitative measurement of ablation crater depth and geometry to a vertical resolution of 0.176 µm. The cross-sectional depth of each crater was derived from five different linear transect measurements, conducted in differing orientations. The representative depth of an individual crater is given by the mean of these separate measurements (n = 5) and its associated uncertainty is derived from the range in measured values. A total of 20 craters were measured in this manner for every sample analysed to determine the mean resultant depth for a sample set. The uncertainty associated with these values was propagated by quadrature.

2.2. Pre-treatment and sample preparation

Thermal pre-treatment by annealing was conducted on a sub-set of samples (summarised in Table 2), to investigate the effect heat-treatment on resultant crater morphologies. Samples were heat-treated at either 850 °C for 48 h, or at 1100 °C for 96 h (Mattinson, 2005; Nasdala et al., 2006). Where a heat-treated sample was being analysed, a primary reference having received the same heat-treatment was used as an external standard.

Regardless of whether a thermal pre-treatment was conducted, it is necessary to ensure all sample surfaces are as clean as possible prior to analysis. Surface contamination (i.e., *common*-Pb) is a concern when sampling such low volumes of material. All samples were subject to several rounds of sonication and rinsing prior to being mounted in a two-part epoxy resin mount. After mounting and polishing, the mount was subject to a further round of cleaning, which involved; (1) several seconds rinsing with ethanol, (2) sonication in a sealed, ethanol filled vessel for 30 min, (3) rinsing with high-purity water, (4) sonication in sealed, high-purity water filled vessels for 30 min, (5) further rinsing with high-purity water, and (6) dried using electronics-safe, pressurised air. Similar care was taken to clean the ablation cell prior to the start of each analytical session.

2.3. Analytical procedure and timeline

All analytical sessions were structured with a sample-standard-bracket technique consisting of five primary reference standard analyses on either side of 10 validation sample analyses (treated as "unknown"), until a total of 20 "unknown" analyses were conducted (i.e., 5-10-5-10-5). Each sample received a total of either 10 or 30 single-shots in sequence before moving onto the next location/sample. Where possible, laser spots were placed in order to avoid any cracks or inclusions visible on the sample surface.

During a TRA, a baseline determination was made for up to 30 s prior to opening the laser shutter. During this time interval, the laser is continually fired at a repetition rate of 4 Hz against the laser shutter, to thermally stabilise or 'warm up' the laser head. The laser shutter opens

Table 1
Instrument set-up and operational parameters.

Laboratory and sample mount preparation	
Laboratory name(s)	Midwest Isotope and Trace Element Research Analytical Center (MITERAC), University of Notre Dame, USA; iCRAG lab, Trinity College Dublin, Ireland.
Sample type/mineral	Polished zircon
Sample preparation	Conventional mineral separation where appropriate, 25 mm round resin mount, polished to ¼ μm finish

Laser ablation system	
Make, model and type	ESI/New Wave Research, UP-213 solid state laser, Nd:YAG
Wavelength (λ)	213 nm
Pulse width	3 ns
Fluence	$\sim$3 Jcm^{-2}
Repetition rate	1 Hz
Spot size	40 μm
Shot count	10 or 30
Sampling mode/pattern	Sequential single shot, static spot ablation
Washout interval	3 s

Transport regime and sweep gas flow	
Laser cell volume	standard 'quick-change drawer' cell ($\sim$8 cm^3)
Transport tubing dimension	200 cm $\times$ 0.48 cm (ID) of Teflon lined Tygon® tubing
Cell atmosphere and transport gas composition	100% He in cell, Ar auxiliary gas combined via 'Y'-style connection 20 cm before entry into the ICP source
Sweep gas flow	1 Lmin^{-1} (He)
Auxiliary gas flow	3 Lmin^{-1} (Ar) at 110 °C, maintained by a CETAC Aridus II desolvating nebuliser, nebuliser pressure 27.8 psi

ICP-MS instrument	
Make, model and type	Nu Instruments, Nu Attom HR-ICP-MS, magnetic sector single collector
Detector mode	Static/parked magnet, peak jump detector mode, combined with FastScan Ion optics
Forward RF power	1300 W
Reflected power	$\leq$3 W
Sweeps	10
Cycles	2500 (for a 10 shot analysis) or 10,000 (for a 30 shot analysis)
Dwell time	500 μs on each isotope
Measured masses	202, 204, 206, 207, 208, 235, 238

Data processing	
Gas blank/baseline duration	Minimum 30 s
Calibration strategy	91500 was used as primary reference standard in brackets of n = 5 either side of validation samples (n = 10), except when Plešovice was used.
Data processing and plotting package(s)	Python based script add-ons operating within Nu Instruments, Nu Quant software platform; in-house Microsoft Excel© spreadsheet; IsoplotR online (Vermeesch, 2018)
Common-Pb correction	No common-Pb correction applied
LIEF correction	No LIEF correction applied
Uncertainty level and propagation	Ages are quoted at 2σ absolute, uncertainty propagation is by quadratic addition.

Table 2
Sample names, ages and pre-treatment descriptions for each of the studied samples. *Annealed sets of a given sample are labelled with an (850/48) or (1100/96) suffix pursuant to the treatment they received (e.g., DD85-17 (850/48) was heat treated at 850 °C for 48 h). Untreated samples are labelled with a (U) suffix.

Sample name*	Pre-treatment	Reference material information
91500 (U)	Untreated	91500 (Wiedenbeck et al., 1995)
91500 (850/48)	850 °C for 48 h	
91500 (1100/96)	1100 °C for 96 h	
Plešovice (U)	Untreated	Plešovice (Sláma et al., 2008)
Plešovice (850/48)	850 °C for 48 h	
Plešovice (1100/96)	1100 °C for 96 h	
DD85-17 (U)	Untreated	DD85-17 Mafic Tonalite, Marmion batholith (Tomlinson et al., 2003)
DD85-17 (850/48)	850 °C for 48 h	
DD85-17 (1100/96)	1100 °C for 96 h	
DD81-29 (U)	Untreated	DD81-29 Heronry Lake Diorite Intrusion (Davis and Edwards, 1986)
DD81-29 (850/48)	850 °C for 48 h	
DD81-29 (1100/96)	1100 °C for 96 h	
WRS-1348 (U)	Untreated	WRS-1348 (Pointon et al., 2012)
Fish Canyon Tuff (U)	Untreated	Fish Canyon Tuff Zircon (Bachmann et al., 2007)

for 1 s to allow a single (1 Hz) shot to strike the focussed sample surface, a 3 s washout interval then follows allowing a partial return to baseline of the signal before the next laser shot. This partial return towards baseline is crucial as it maintains an elevated signal intensity whilst also allowing the *NICE script* Nu-Quant software add-on to decipher signal peaks. This cycle of firing and washout continues until either 10 or 30 consecutive laser shots have been fired in the same location. The duration of a multi-shot analysis conducted in this manner is ~3 to 8 min depending on the total shot count applied. A standard bracketed analytical session consisting of several such multi-shot analyses (n = 35) therefore, can take up to between 2 and 5 h. It should be noted that no pre-ablation shot or raster procedure was undertaken in this study to 'clean' the sample of potential surface common Pb contamination, as the ^{204}Pb ion signal remained below the limit of quantification (LOQ) throughout each analysis. As a precautionary measure the first 10% of shots are ignored within the Nu Quant software to avoid any potential for ^{204}Pb surficial contamination, but can still be integrated as part of the TRA at the user's discretion.

2.4. Signal integration and data reduction

Nu Quant is Nu Instruments software developed for processing data obtained using the Attom HR-ICP-MS. It allows the user to construct batch files containing several separate TRA files. Single and multi-shot analyses require each TRA to be processed using a *NICE script* add-on, which operates within the Nu Quant software platform. The Nu Quant software platform offers the freedom for users to construct and import their own Python-based *NICE scripts* for data reduction purposes. Two *NICE script* variants were developed for the purposes of multi-shot data reduction; version 2 (*v.2*), which utilises user defined ^{238}U signal threshold values to determine the start and end of each laser shot; and version 5 (*v.5*), whereby the software delineates signal pulses between the start of the signal for the first shot and the end of the signal for the final shot. Both require the user to input multiple parameters before the signals can be compiled. These iterations of the script contained the most robust algorithms tested within this study and are freely available as supplementary material.

2.4.1. Version 2 (v.2)

The start and end points of the 30s baseline/'gas-blank' measurement (acquired prior to firing the laser) are defined by the user in terms of "baseline start cycle" and "baseline end cycle", respectively. This selection of baseline continuum signal is used to subsequently perform a baseline subtraction calculation of the net acquired signal intensities. Ideally therefore, users should select as much of a representative baseline signal as possible. The user must also determine the "start peak trigger", a threshold value for the ^{238}U ion signal, which will define the start and end points of signal peaks. To avoid falsely triggering and integrating signal peaks too narrow to be real (i.e., signal noise), the user defines the minimum *channel width*, which constitutes a real peak. When necessary, the user can request that the software ignore the first number of shots/peak during ratio computation so as to avoid integrating signals potentially affected by surface common-Pb contamination. Cycles satisfying the conditions defined by the user (i.e., above the minimum triggering threshold, based on ^{238}U ion signal intensity; and of sufficient channel width) are integrated as part of a multi-shot analysis. Ratios are calculated for a single peak by summing the total number of counts for each isotope across the entire *peak width*, and applying a subtraction of the baseline average counts (for the same isotope) to this value. A summary of the data handling process for *v.2* is given in Fig. 1.
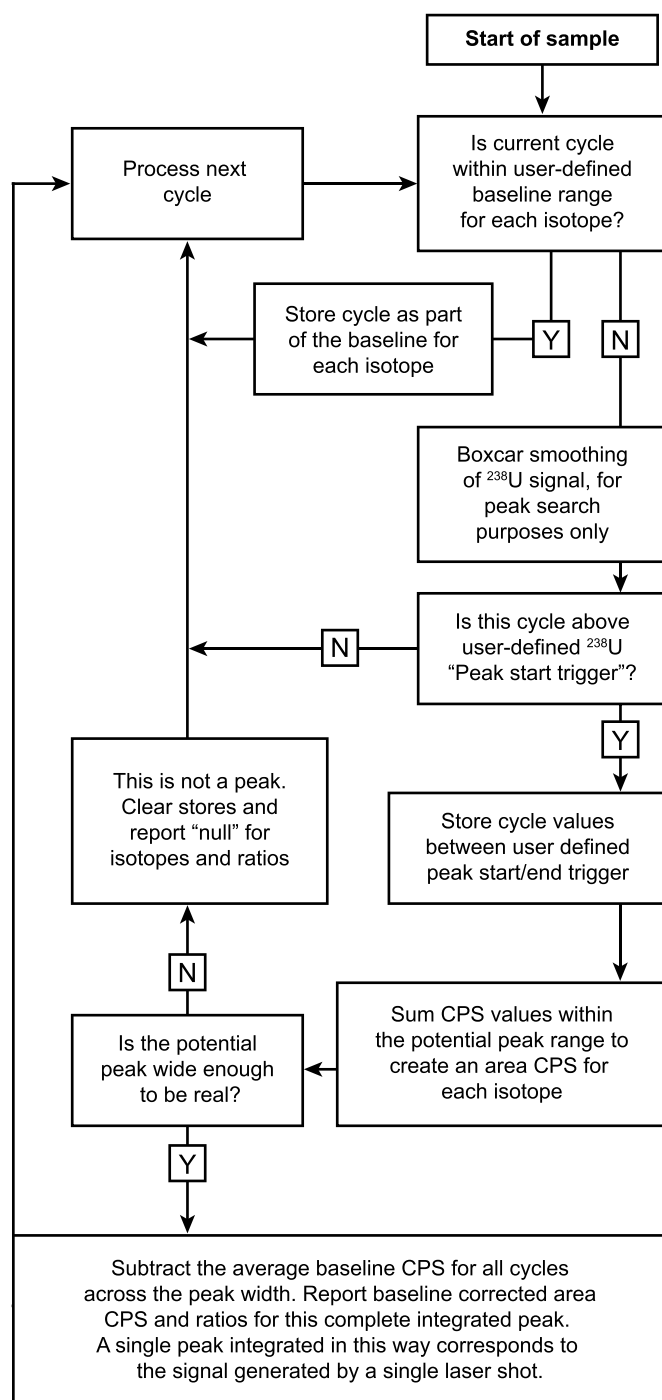

Fig. 1. The operational workflow undertaken to crop and integrate 'peak tops' within the *NICE script v.2*.

2.4.2. Version 5 (v.5)

Version 5 of the *NICE script* add-on was used in this study when the cumulative counts on the least abundant isotope measured in a ratio pair (usually ^{207}Pb) integrated over the course of an analysis were low (i.e., for analyses of 10 shots and Fish Canyon Tuff (U); see Section 3.4). Version 5 does not operate using a trigger value based on ^{238}U ion signal intensity to initiate a *peak search*. Instead the user defines the first and last cycles within a TRA that pertain to an on-peak measurement.
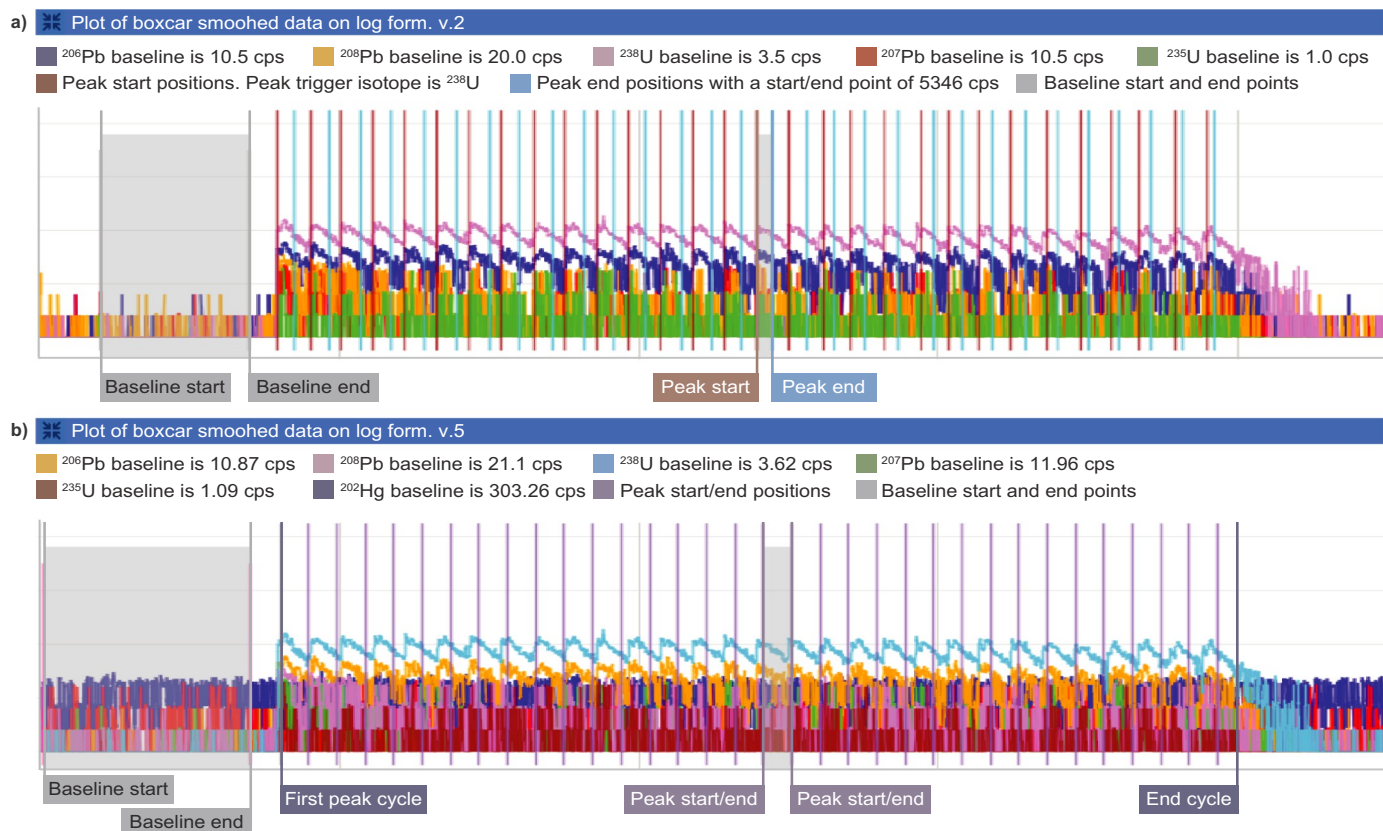
Fig. 2. Representative TRAs as displayed (with annotation) within the Nu-Quant software of both *NICE script* add-ons for the same 91500 zircon analysis. (a) Version 2 (v.2) was used for data reduction of 30 shot analyses in this contribution, with the exception of Fish Canyon Tuff (U). This version operates by integrating peaks above a threshold 'peak trigger' based on ^{238}U ion signal intensity for a fixed channel width as defined by the user. This effectively operates to crop peak-tops only, ignoring cycles not satisfying user defined thresholds. (b) Version 5 (v.5) was used to integrate analyses of 10 shots and Fish Canyon Tuff (U), where there are fewer cumulative counts to integrate for each isotope. No ion signal intensity dependent peak search function operates in v.5, instead the user defines the first cycle pertaining to the onset of signal pulses and the last. The software then divides the intervening cycles into equal channel widths for integration. The alignment of these fixed width integrations is made difficult with within-run variation in washout efficiency.

Back-to-back peak brackets of a user defined width then divide the space between the first and last peak for an entire TRA. A representative TRA for both *NICE script* versions are illustrated in Fig. 2.

2.5. Linear drift and mass bias correction

Data processing including correction of instrumental drift and mass bias, as well as uncertainty propagation were carried out using an 'in-house' Microsoft Excel© spreadsheet developed after Simonetti et al. (2005). Mean normalisation factors were calculated for each of the three standard brackets, sensu Fisher et al. (2010). These normalisation factors were multiplied into each integrated ratio for the sample data by fractional degrees, weighted according to their '*within-run*' position relative to the standard brackets to correct for instrumental drift and mass bias during the course of an analytical session.

2.6. Uncertainty propagation and data rejection

All potential sources of uncertainty were propagated into individual ratio determinations, including those related to the external reproducibility of the primary reference material. No common Pb or LIEF corrections were applied to data reported here. In all cases ^{207}Pb/^{235}U ratios were calculated using the ^{238}U/^{235}U constant of 137.88 (Steiger and Jäger, 1977) and all ages were calculated using the decay constants of Jaffey et al. (1971).

Prior to plotting, any acquired data that produced Rho error correlations > 1 were rejected. For those samples overlapping the Concordia curve, an additional rejection was applied based upon percent discordance, whereby data exceeding user defined thresholds are excluded (usually data ≥ 20% discordance are rejected). For those data plotting as discordant arrays, the rejection of data was conducted on a visual basis by the user. All Concordia plots were constructed using IsoplotR (Vermeesch, 2018) and uncertainties therein are reported at the 2σ level.

3. Results

3.1. External precision

Both 91500 (1065.4 ± 0.6 Ma; Wiedenbeck et al., 1995) and Plešovice (337.13 ± 0.37 Ma; Sláma et al., 2008) were used as primary reference zircon standards during the course of this study. The reproducibility (2SD%) of both external reference standards regardless of the pre-treatment they received is < 7.5% and < 5.5% for ^{207}Pb/^{206}Pb and ^{206}Pb/^{238}U, respectively for 30 shot ablations. For analyses employing 10 shots, the reproducibility (2SD%) of both external reference standards is < 22.5% and < 5% ^{207}Pb/^{206}Pb and ^{206}Pb/^{238}U, respectively. These ratio value determinations were made over the course of several analytical sessions, which were conducted over the course of several days, as summarised in Table 3.

Table 3

External reproducibility (2SD%) of baseline subtracted raw ratios achieved for all primary reference standards used within this study.

External reference standard	n	$^{207}Pb/^{206}Pb$ (2SD%)	$^{206}Pb/^{238}U$ (2SD%)
30 shot analyses			
91500 (U)	n = 80	6.0	4.8
91500 (850/48)	n = 79	6.1	4.9
91500 (1100/96)	n = 49	7.4	4.0
Plešovice (U)	n = 35	6.1	3.9
Plešovice (850/48)	n = 35	7.2	5.4
Plešovice (1100/96)	n = 15	5.7	1.9
10 shot analyses			
91500 (U)	n = 55	22.2	4.9
Plešovice (U)	n = 46	16.1	4.2

3.2. Internal precision

The internal precision of all measured samples within a given analytical session is summarised in Table 4. The 'within-run' reproducibility (2SD%) of all samples receiving 30 shots, regardless of the pre-treatment they received is < 2.4% and < 1.6% for $^{207}Pb/^{206}Pb$ and $^{206}Pb/^{238}U$ respectively, with the exception of Fish Canyon Tuff zircon (U). The relatively low abundance of radiogenic Pb in Fish Canyon Tuff zircon (28.37 ± 0.05 Ma; Bachmann et al., 2007) reduces the precision achievable for a 30 shot analysis (see Table 4), regardless of the *NICE script* used to generate integrations. For analyses of 10 shots, the reproducibility (2SD%) of untreated samples measured is < 3.9% and < 1.4% for $^{207}Pb/^{206}Pb$ and $^{206}Pb/^{238}U$, respectively. These ratio determinations were made during the same analytical sessions for each sample set. Thermal annealing pre-treatment does not improve internal precision.

Table 4

Internal reproducibility (2SD%) uncorrected ratios achieved (n = 20) for all samples analysed. Those analyses reduced using NICE script v.5 are highlighted with an asterisk (*).

Sample	$^{207}Pb/^{206}Pb$ (2SD%)	$^{206}Pb/^{238}U$ (2SD%)
91500 (U)	0.64	0.39
91500 (850/48)	0.73	0.35
91500 (1100/96)	0.63	0.49
Plešovice (U)	0.59	0.42
Plešovice (850/48)	0.81	0.51
Plešovice (1100/96)	0.66	0.26
DD81-29 (U)	0.92	1.56
DD81-29 (850/48)	0.34	0.64
DD81-29 (1100/96)	0.31	0.84
DD85-17 (U)	0.68	0.98
DD85-17 (850/48)	0.86	1.15
DD85-17 (1100/96)	0.32	0.93
WRS-1348 (U)	2.35	0.86
Fish Canyon Tuff (U)*	29.41	4.83
91500 (U)*	3.82	0.53
Plešovice (U)*	2.31	0.27
WRS-1348 (U)*	3.00	1.36

3.3. Age determinations of validation samples

The samples utilized to demonstrate the validity of the multi-shot technique outlined herein all have independently verified ID-TIMS ages. All samples regardless of the pre-treatment they received have calculated ages consistently reproducible to within ≤1% of their published age, with the exception of Fish Canyon Tuff (1.34%). All are within an acceptable range of MSWD values (Spencer et al., 2016). All age plots are included in Fig. 3.

The weighted mean age data (Table 5) regardless of heat treatment applied reproduce to within < 1.57% of their published U-Pb ID-TIMS
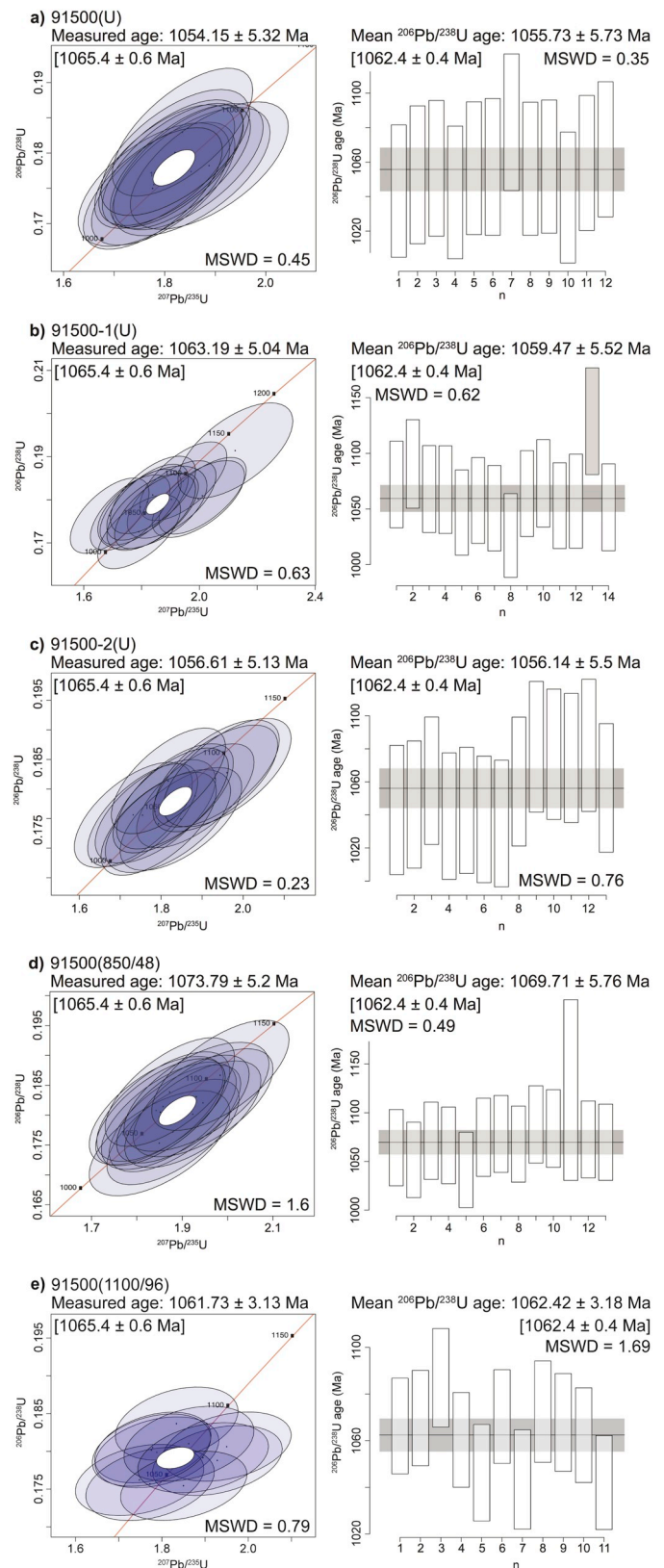
Fig. 3. Age data are displayed both in Wetherill Concordia space and as weighted mean age plots. Uncertainties are quoted at a 2σ level (95% confidence). Plots were generated using IsoplotR (Vermeesch, 2018). All plots having blue ellipses were reduced using *NICE script v.2* and consist of 30 shot analyses. Plots containing red ellipses were reduced using *NICE script v.5* and consist of 10 shot analyses, with the exception of plot (j) Fish Canyon Tuff (U). (For interpretation of the references to colour in this figure legend, the reader is referred to the web version of this article.)
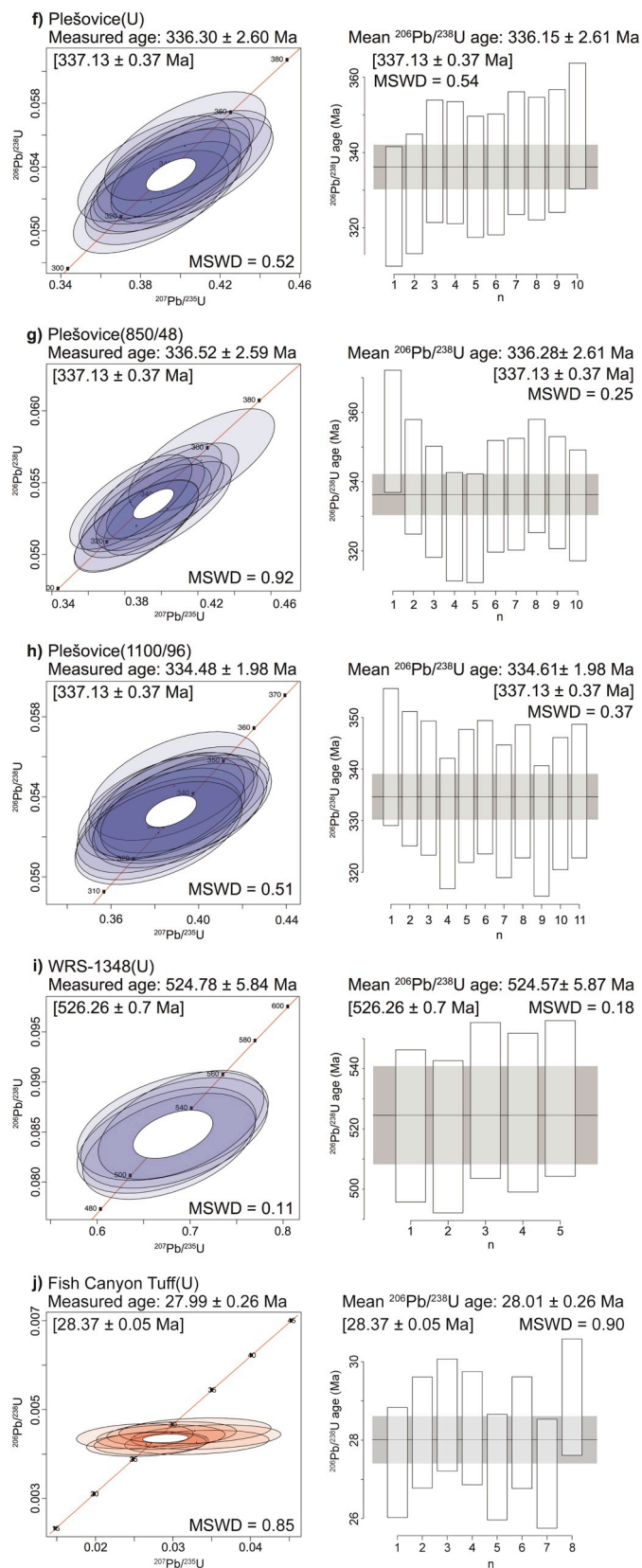
f) Plešovice(U)
Measured age: 336.30 ± 2.60 Ma
[337.13 ± 0.37 Ma]

Mean ^{206}Pb/^{238}U age: 336.15 ± 2.61 Ma
[337.13 ± 0.37 Ma]
MSWD = 0.54

g) Plešovice(850/48)
Measured age: 336.52 ± 2.59 Ma
[337.13 ± 0.37 Ma]

Mean ^{206}Pb/^{238}U age: 336.28± 2.61 Ma
[337.13 ± 0.37 Ma]
MSWD = 0.25

h) Plešovice(1100/96)
Measured age: 334.48 ± 1.98 Ma
[337.13 ± 0.37 Ma]

Mean ^{206}Pb/^{238}U age: 334.61± 1.98 Ma
[337.13 ± 0.37 Ma]
MSWD = 0.37

i) WRS-1348(U)
Measured age: 524.78 ± 5.84 Ma
[526.26 ± 0.7 Ma]

Mean ^{206}Pb/^{238}U age: 524.57 ± 5.87 Ma
[526.26 ± 0.7 Ma]   MSWD = 0.18

j) Fish Canyon Tuff(U)
Measured age: 27.99 ± 0.26 Ma
[28.37 ± 0.05 Ma]

Mean ^{206}Pb/^{238}U age: 28.01 ± 0.26 Ma
[28.37 ± 0.05 Ma]   MSWD = 0.90

k) DD81-29 (U)
Intercept age: 2713.7 ± 45.2 Ma
[2701 ± 1.2 Ma]

Mean ^{207}Pb/^{206}Pb age: 2710.9 ± 15.7 Ma
[2701 ± 1.2 Ma]   MSWD = 0.29

l) DD81-29 (850/48)
Intercept age: 2698.3 ± 22.6 Ma
[2701 ± 1.2 Ma]

Mean ^{207}Pb/^{206}Pb age: 2700.4 ± 10.9 Ma
[2701 ± 1.2 Ma]
MSWD = 0.40

m) DD81-29 (1100/96)
Intercept age: 2693.7 ± 85.2 Ma
[2701 ± 1.2 Ma]

Mean ^{207}Pb/^{206}Pb age: 2678.4 ± 24.2 Ma
[2701 ± 1.2 Ma]
MSWD = 0.10

n) DD85-17 (U)
Intercept age: 3001.5 ± 31.3 Ma
[3001.6± 3.4 Ma]

Mean ^{207}Pb/^{206}Pb age: 3007.5 ± 18.2 Ma
[3001.6 ± 3.4 Ma]   MSWD = 0.13

o) DD85-17 (850/48)
Intercept age: 3003.8 ± 34.1 Ma
[3001.6 ± 3.4 Ma]

Mean ^{207}Pb/^{206}Pb age: 2999.9 ± 11.8 Ma
[3001.6 ± 3.4 Ma]

Fig. 3. (*continued*)   **Fig. 3.** (*continued*)

ages for analyses of 30 shots. Moreover, most samples typically reproduce to within ≪1% of their published ages. Analyses conducted using 10 shots and reduced using *NICE script version 5* (*v.5*) yield weighte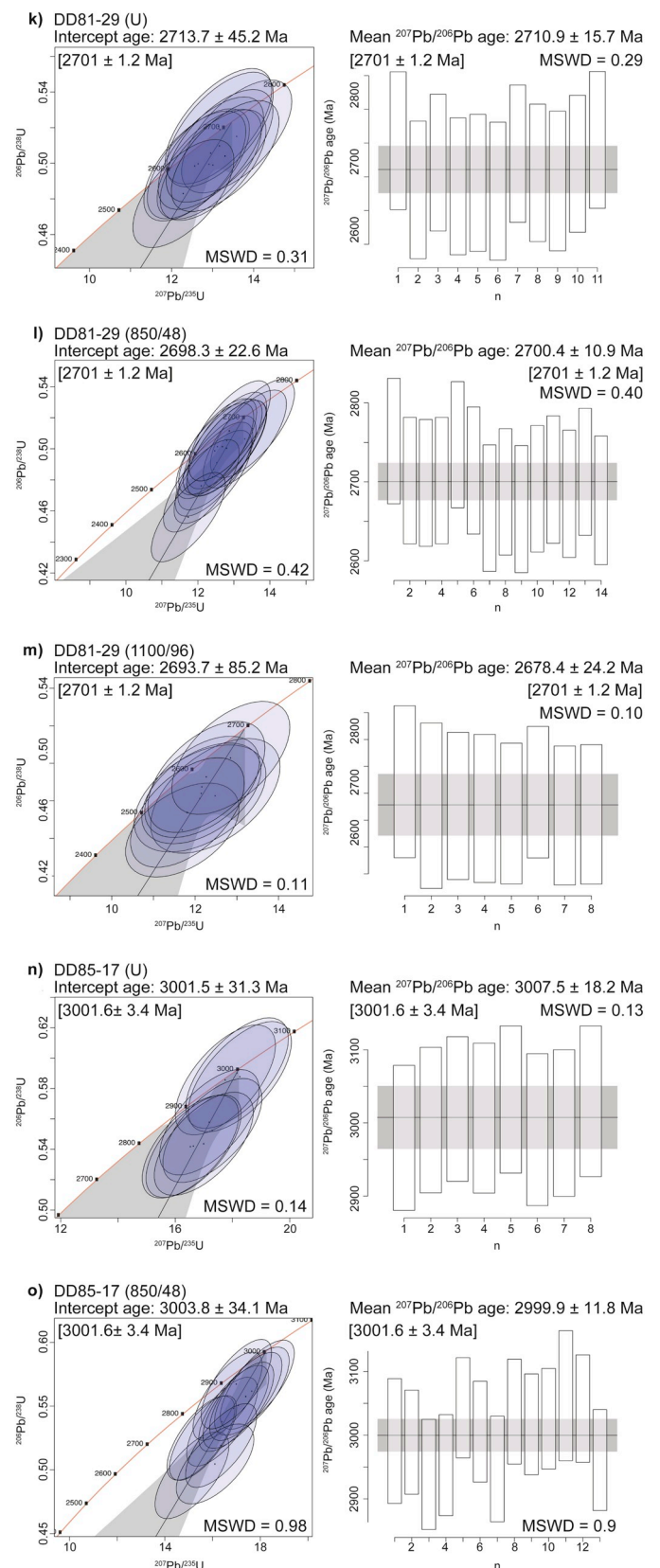d mean ages that are reproducible to within < 0.82% of their accepted ages on samples of untreated 91500, Plešovice, and WRS-1348 zircons. All U-Pb results for samples analysed here are displayed both in Concordia diagrams and in weighted mean plots (Fig. 3) demonstrating both the accuracy and precision achieved by the multi-shot LA-ICP-MS
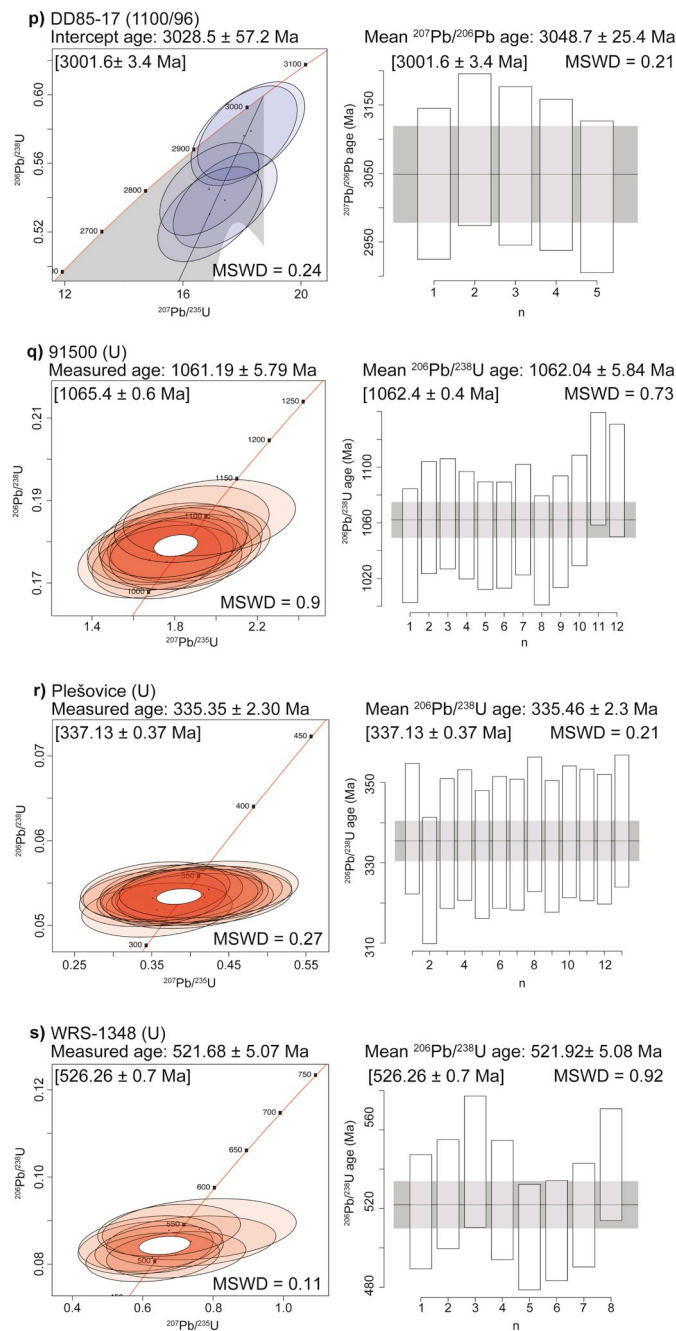
p) DD85-17 (1100/96)
Intercept age: 3028.5 ± 57.2 Ma
[3001.6± 3.4 Ma]

Mean ^{207}Pb/^{206}Pb age: 3048.7 ± 25.4 Ma
[3001.6 ± 3.4 Ma]   MSWD = 0.21

MSWD = 0.24

q) 91500 (U)
Measured age: 1061.19 ± 5.79 Ma
[1065.4 ± 0.6 Ma]

Mean ^{206}Pb/^{238}U age: 1062.04 ± 5.84 Ma
[1062.4 ± 0.4 Ma]   MSWD = 0.73

MSWD = 0.9

r) Plešovice (U)
Measured age: 335.35 ± 2.30 Ma
[337.13 ± 0.37 Ma]

Mean ^{206}Pb/^{238}U age: 335.46 ± 2.3 Ma
[337.13 ± 0.37 Ma]   MSWD = 0.21

MSWD = 0.27

s) WRS-1348 (U)
Measured age: 521.68 ± 5.07 Ma
[526.26 ± 0.7 Ma]

Mean ^{206}Pb/^{238}U age: 521.92± 5.08 Ma
[526.26 ± 0.7 Ma]   MSWD = 0.92

MSWD = 0.11

Fig. 3. (*continued*)

approach adopted here.

3.4. NICE script comparison

Signal integration by either *NICE* data reduction script will be inhibited when the least abundant isotope measured in a ratio pair (i.e., ^{207}Pb) fails to exceed (or remains close to) the LOQ. Fish Canyon Tuff (U) zircon has a relatively low abundance of radiogenic Pb (i.e. < 5 ppm; Bachmann et al., 2007), and is therefore ideally suited when comparing the efficacy of both *NICE script v.2* and *v.5* for samples and/ or shot counts yielding lower signal intensities.

A 30 shot analysis of Fish Canyon Tuff (U) was processed in the first instance using *NICE script v.2*, which operates to sub-sample integrations (described in detail in Section 2.4.1). This effective 'peak-top'

cropping reduces the counts integrated for each laser pulse for each isotope, consequently ^{207}Pb ion signals are for the most part below the LOQ. When plotted in Tera-Wasserberg space (Fig. 4a), calculated U/Pb ratios display apparent "Pb gain" effects and/or interferences on mass 204. The ion signal for mass 204 remains below LOQ for both *NICE script* versions however. Consequently, surface contamination by common Pb cannot be invoked to explain the apparent "Pb gain" observed when reducing the data using *NICE script v.2*. Instead, this effect is wholly artificial, being an artefact of poor counting statistics on mass 207.

NICE script v.5 by contrast integrates the entirety of a signal pulse. By processing a TRA with the latter script, the resultant counts for a given laser pulse exceed the LOQ for mass 207 and consequently ^{206}Pb/^{238}U and ^{207}Pb/^{235}U remain unaffected by poor counting statistics (Fig. 4b). This highlights the utility of *NICE script v.5* when low ion signals are recorded for either for young zircons, such as Fish Canyon Tuff and/or for analyses of < 30 shots.

Analyses conducted using a shot count of 10 also encountered problems associated with low Pb ion signals where data reduction was conducted in the 'peak-top' cropping fashion of the *NICE script v.2*. Thus, for these analyses *NICE script v.5* was used instead. Analyses of 10 shots reduced in this way reproduce to within < 0.87% of their accepted concordia ages based on analyses of untreated 91500, Plešovice, and WRS-1348. More accurate weighted mean ages result from reducing the entirety of a peak as with *NICE script v.5* for analyses yielding low signal counts; however, external reproducibility suffers as a result (see Table 3). *NICE script v.2*. should be utilised preferentially when analysing samples either with a high abundance of Pb or when using a shot count > 10.

3.5. Monitoring time-dependent fractionation

The degree of time-dependent 'downhole' fractionation occurring during a single laser ablation analysis is determined by monitoring the variability of the measured ^{206}Pb/^{238}U ratio on a shot-to-shot basis. Where time-dependent fractionation of ^{206}Pb over a relatively more refractory ^{238}U has occurred during ablation, an increasing trend in measured ^{206}Pb/^{238}U would be expected on a shot-to-shot basis as the ablation crater deepens. Calculating the degree of time-dependent fractionation over the course of an analysis can be made by dividing the mean ^{206}Pb/^{238}U ratio of the first half of an analysis by its corresponding second segment. This calculation constitutes a fractionation index (FI). A FI of near unity suggests a minimal degree of time-dependent fractionation has occurred over the course of an analysis. Fig. 5 charts the variability of the ^{206}Pb/^{238}U ratio on a shot-to-shot basis over the course of various representative analyses of both 30 and 10 shots (Fig. 5. a and b, respectively). No discernible trend of increase exists for ^{206}Pb/^{238}U measured between shots over the course of an individual analysis and all have a FI near unity, suggesting minimal time-dependent 'downhole' fractionation has occurred.

3.6. Sample volume estimates

Individual crater depth measurements and their associated uncertainties are derived from repeated cross-sectional transects (n = 5) of the pit diameter viewed using WLI. Mean crater depth, depth variability and mean ablated volume estimates are summarised in Table 6 for each sample set (n = 20). Estimates for the ablated volume assumes a cylindrical crater geometry and 100% transport efficiency of the analyte to the ICP source (i.e., no sample re-deposition or loss within the transfer line to the ICP). The calculated depth achieved per laser pulse is between 47 nm and 70 nm, depending on the target sample.

Fig. 6a and b are based a representative WLI analysis of Plešovice

Table 5

Summary of age data illustrated in Fig. 3. Accepted ages for each sample are highlighted in bold. 91500 zircon was used as the primary reference standard for all analyses with the exception of those 91500 samples where Plešovice was used instead. Weighted mean ages are based on $^{206}Pb/^{238}U$ ratios for zircons younger than 1100 Ma, otherwise the mean $^{207}Pb/^{206}Pb$ age is adopted for reference.

Sample name	Measured age (Ma)	Reproducibility (%)	MSWD	n	Weighted mean age (Ma)	Reproducibility (%)	MSWD	n	NICE script version
30 shot analyses									
91500	1065.4 ± 0.6				1062.4 ± 0.4				
Wiedenbeck et al., 1995									
91500 (U)	1054.15 ± 5.32	1.06	0.45	12	1055.73 ± 5.73	0.11	0.35	12/12	v.2
91500-1 (U)	1063.19 ± 5.04	0.21	0.63	14	1059.47 ± 5.52	0.28	0.62	13/14	v.2
91500-2 (U)	1056.61 ± 5.13	0.83	0.23	13	1056.14 ± 5.5	0.59	0.76	13/13	v.2
91500 (850/48)	1073.79 ± 5.2	0.79	1.6	13	1069.71 ± 5.76	0.69	0.49	13/13	v.2
91500 (1100/96)	1061.73 ± 3.13	0.34	0.79	11	1062.42 ± 3.18	0.002	1.69	11/11	v.2
Plešovice	337.13 ± 0.37				337.13 ± 0.37				
Sláma et al., 2008									
Plešovice (U)	336.30 ± 2.6	0.25	0.52	10	336.15 ± 2.61	0.29	0.54	10/10	v.2
Plešovice (850/48)	336.52 ± 2.59	0.18	0.92	10	336.28 ± 2.61	0.88	0.25	10/10	v.2
Plešovice (1100/96)	334.48 ± 1.98	0.79	0.51	11	334.61 ± 1.98	0.75	0.37	11/11	v.2
DD81-29	2701 ± 1.2				2701 ± 1.2				
Davis and Edwards, 1986									
DD81-29 (U)	2713.7 ± 45.2	0.47	0.31	11	2710.9 ± 15.7	0.37	0.29	11/11	v.2
DD81-29 (850/48)	2698.3 ± 22.6	0.10	0.42	14	2700.4 ± 10.9	0.02	0.40	14/14	v.2
DD81-29 (1100/96)	2693.7 ± 85.2	0.27	0.11	8	2678.4 ± 24.2	0.84	0.10	8/8	v.2
DD85-17	3001.6 ± 3.4				3001.6 ± 3.4				
Tomlinson et al., 2003									
DD85-17 (U)	3001.5 ± 31.3	0.003	0.14	8	3007.5 ± 18.2	0.20	0.13	8/8	v.2
DD85-17 (850/48)	3003.8 ± 34.1	0.07	0.98	13	2999.9 ± 11.8	0.06	0.90	13/13	v.2
DD85-17 (1100/96)	3028.5 ± 57.2	0.90	0.24	5	3048.7 ± 25.4	1.57	0.21	5/5	v.2
WRS-1348	526.26 ± 0.7				526.26 ± 0.7				
Pointon et al., 2012									
WRS 1348 (U)	524.78 ± 5.84	0.28	0.11	5	524.57 ± 5.87	0.32	0.18	5/5	v.2
Fish Canyon Tuff	28.37 ± 0.05				28.37 ± 0.05				
Bachmann et al., 2007									
Fish Canyon Tuff (U)	27.99 ± 0.26	1.34	0.85	8	28.01 ± 0.26	1.27	0.90	8/8	v.5
10 shot analyses									
91500	1065.4 ± 0.6				1062.4 ± 0.4				
Wiedenbeck et al., 1995									
91500 (U)	1061.19 ± 5.79	0.40	0.9	12	1062.04 ± 5.84	0.03	0.73	12/12	v.5
Plešovice	337.13 ± 0.37				337.13 ± 0.37				
Sláma et al., 2008									
Plešovice (U)	335.35 ± 2.30	0.53	0.27	13	335.46 ± 2.3	0.50	0.21	13/13	v.5
WRS-1348	526.26 ± 0.7				526.26 ± 0.7				
Pointon et al., 2012									
WRS-1348 (U)	521.68 ± 5.07	0.87	0.11	8	521.92 ± 5.08	0.82	0.92	8/8	v.5

(U), with a cross-section comparison of 30 and 10-shot craters. Small-scale inhomogeneous sampling at the crater floor is evidenced in Fig. 6a, which is exaggerated in its vertical dimension. The alternate plan view offered by Fig. 6b, demonstrates the lateral extent of this sampling inhomogeneity. The effect is less pronounced for 10-shot craters.

A qualitative comparison of laser matter interaction is shown by secondary electron images. Fig. 6c and c' illustrates a crater produced by static high frequency ablation (5 Hz, 20 s), with all other parameters being maintained as they are for the multi-shot approach described herein. It has been included as a point of comparison between craters produced by 30 and 10-shots (Fig. 6d-d' and e-e', respectively) in the same target matrix (i.e., a single fragment of 91500 (U)). The relative depth, degree of welding and re-deposition is clearly reduced (albeit not eliminated) where fewer shots are applied. The 1:1 scaling of secondary electron imaging also emphasises the much-reduced aspect ratio of craters produced by the multi-shot approach adopted in this study.
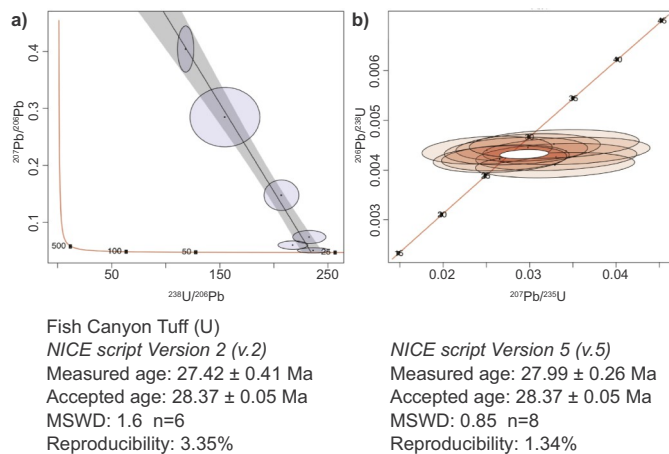
Fig. 4. A comparison of age data generated for the same 30 shot analysis of Fish Canyon Tuff (U) zircon using (a) NuQuant *NICE script v.2* plotted in Tera-Wasserberg space and (b) *NICE script v.5* plotted in Wetherill Concordia space. Uncertainties are quoted at a 2σ level with a confidence interval of 95%. Plots were generated using IsoplotR (Vermeesch, 2018).

3.7. Thermal annealing

Marillo-Sialer et al. (2016) demonstrated that the rate of ablation of a zircon matrix is at least partially controlled by the crystalline order of its lattice. Thermal annealing was investigated as a means by which to exercise some degree of control over ablation rate (depth) of the target matrix and the geometry of the resultant craters. The WLI data (summarised in Table 6) demonstrate little utility of thermal annealing as a pre-treatment in limiting resultant crater depths following multi-shot ablation. The variable behaviour of crater excavation was assessed by calculating the standard deviation of the resultant crater depths for a given sample set. The variability (2SD%) of crater depths for any given sample set is < 31.2%. Thermally annealed sample sets demonstrated no discernible improvement in variability (2SD%) over their untreated counterparts.

Despite reproducing predominantly to within 1% of their accepted mean ages, the ages calculated for thermally annealed samples often did not overlap (within uncertainty) of their accepted ages. This variability in accuracy would remain difficult to assess for unknowns treated by annealing and analysed by the multi-shot LA-ICP-MS method described here. The most accurate age determinations were made on untreated samples having (for the most part) delivered larger volumes of analyte to the ICP-MS instrument.

4. Discussion

4.1. Accuracy and precision

The accuracy of the multi-shot LA-ICP-MS analytical method reported here is typically within the 1–2% (2σ) level expected for conventional static LA-ICP-MS analysis (Horstwood et al., 2016). The least abundant isotope measured in a ratio pair (i.e., ^{207}Pb in U-(Th)-Pb geochronology) will remain the limiting factor for determining the accuracy and precision of this technique. Consequently, accuracy and precision are inextricably linked to the volume of analyte produced, and therefore both can only be improved at the expense of depth or lateral resolution.

4.2. Thermal annealing as a pre-treatment

Slight variations in optical and thermo-physical properties between zircon matrices due to either radiation damage-induced lattice defects and/or colour will affect the laser–zircon interaction, and thus the
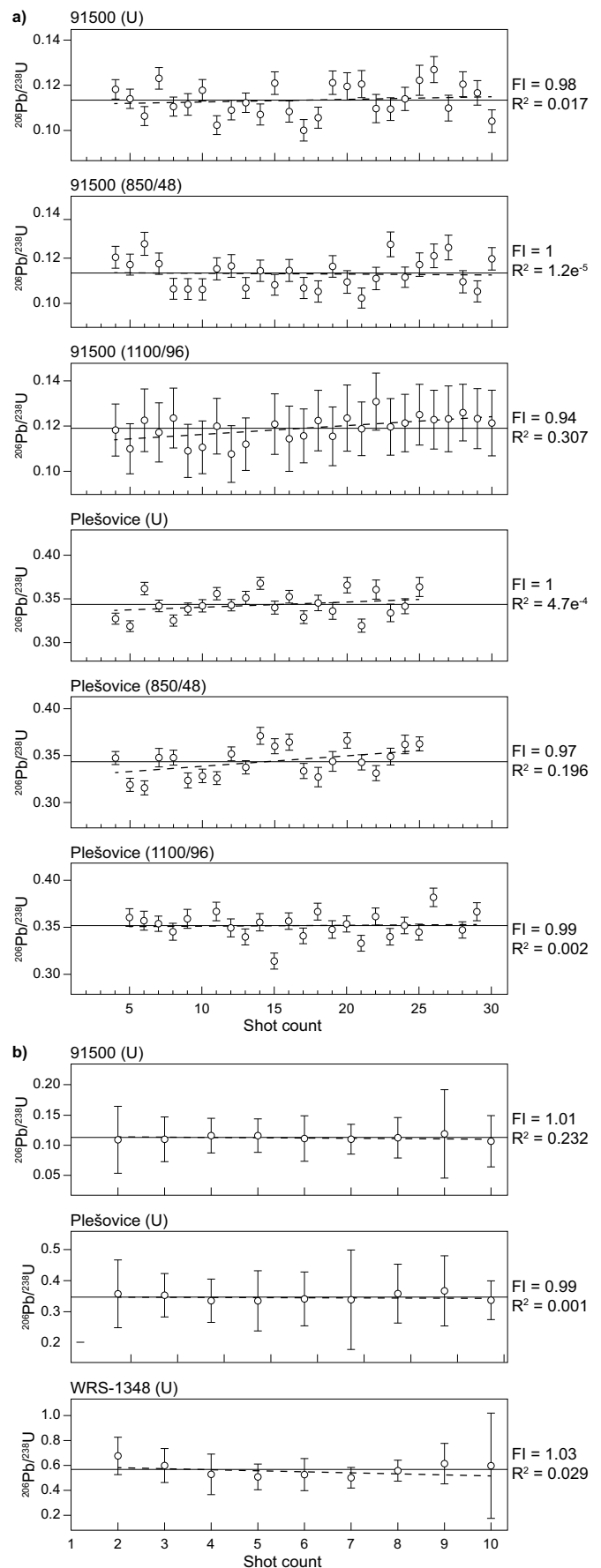
(caption on next page)

Fig. 5. ^{206}Pb/^{238}U variability charted on a shot-to-shot basis for representative analyses of both; (a) 30 and; (b) 10 shots. Examples of heat-treated samples are also shown. Ratio uncertainties are calculated based upon the minimum ^{206}Pb counts received for each individual shot. Little to no ratio variability in the above analyses results in a FI of near unity for each, suggesting time-dependent 'downhole' fractionation has been significantly reduced for crater aspect ratios ≪1.

---

amount of material removed by each laser pulse (Kooijman et al., 2012; Marillo-Sialer et al., 2014). Several previous studies have shown that the rate of ablation of a zircon matrix is at least partially controlled by the order of its crystalline lattice (Allen and Campbell, 2012; Crowley et al., 2014; Marillo-Sialer et al., 2016). The magnitude to which zircon crystal lattice recovery by annealing exhibits control over ablation behaviour was examined over 30 shots in this study.

There is only partial support for the hypothesis put forward by Allen and Campbell (2012) that increasing crystal density via annealing reduces the rate ablation rate of the target analyte. In this study, annealed sample sets almost all demonstrate an increased mean crater depth relative to that of their untreated counterpart, with the notable exception of DD81-29. A reduction in ablation rate therefore, cannot be invoked as a universal behavioural response of annealed zircon matrices. There is also little evidence to suggest that annealing as a pretreatment unifies/homogenises the ablation response of a sample set to incident laser radiation at the spatial scale investigated here. No discernible improvement in crater depth variability for annealed sample sets is observed, again with the exception of DD81-29. The effect of annealing on both crater geometries and/or resulting ages is difficult to assess between sample sets and is therefore not necessary as a pretreatment for the protocol described herein.

4.3. Applications in geochronology

Where natural minerals are concerned, structural and chemical

inhomogeneities are often present yet unresolvable using conventional LA-ICP-MS approaches. By integrating and collating multiple, consecutive single shots it is possible to generate precise ages, which are statistically indistinguishable from dates determined by ID-TIMS. Collating multiple signal pulses in this manner allows for an age determination to be made for as few as 10 shots. Depending on the number of shots applied to the target material, vertical sampling can be conducted from the micron to the sub-micron scale. The ion signals recorded for the least abundant isotope measured (i.e., ^{207}Pb) will remain the limiting factor for vertical resolution of this approach. The laser protocol outlined in this study was designed to be generally applicable to zircon U-Pb work, employing practicable spot sizes and moderate laser fluences. Modifications to this protocol could potentially be employed to maximise ion signals for fewer shots (and hence improve the vertical spatial resolution), alternatively an increased number of shots may be applied to improve the analytical accuracy and precision of the technique described here, so long as a critical aspect ratio of < 1 is maintained in order to minimise LIEF.

5. Conclusions

A multi-shot approach to U-Pb age determinations by LA-ICP-MS allows for precise and often indistinguishable ages compared to those determined by ID-TIMS for the same zircon reference materials and unknowns. The instrumental set-up requires no modification of the standard equipment for both the UP213 laser ablation system and Attom HR-ICP-MS employed here. Moreover, the standard ablation cell allows for the maintenance of elevated signal intensities when utilised in conjunction with a short washout interval between shots. The shallow ablation depths achieved by multi-shot analysis allow for precise age determinations to be made both on the micron to sub-micron scale whilst negating the need to apply a 'downhole' inter-elemental fractionation correction.

Table 6

Data summary of crater morphology and ablation behaviour for several heat treated and untreated zircon matrixes. Mean crater depths (n = 20) as measured by WLI and include analyses of both 30 and 10 shots. *Assuming the specific gravity of zircon to be 4.65 g cm^{-3} (Deer et al., 1992) **Pb concentrations used for approximation are derived from (1) Wiedenbeck et al., 1995; (2) Sláma et al., 2008; (3) Pointon et al., 2012; (4) Bachmann et al., 2007.

Sample name	Mean crater depth (μm)	Crater aspect ratio (depth/diameter)	Crater depth variability (2SD%)	Approx. depth per shot (μm)	Mean ablated volume (μm^3)	Approx. Zircon consumption (ng)*	Approx. Pb consumption (pg)**	
30 shot analyses								
91500 (U)	1.41 ± 0.03	0.04	13.2	0.05	1770 ± 120	8.23	0.11–0.13	(1)
93 (850/48)	1.53 ± 0.06	0.04	19.8	0.05	1930 ± 240	8.97	0.12–0.14	
91500 (1100/96)	1.90 ± 0.08	0.05	22.5	0.06	2390 ± 360	11.1	0.14–0.18	
Plešovice (U)	1.67 ± 0.10	0.04	31.2	0.06	2100 ± 420	9.77	0.21–1.54	(2)
Plešovice (850/48)	1.82 ± 0.06	0.05	16.8	0.06	2290 ± 270	10.65	0.22–1.68	
Plešovice (1100/96)	1.79 ± 0.07	0.04	20.6	0.06	2250 ± 310	10.46	0.22–1.65	
DD81-29 (U)	2.11 ± 0.09	0.05	18.7	0.07	2650 ± 450	12.32	–	
DD81-29 (850/48)	1.99 ± 0.09	0.05	17.9	0.07	2490 ± 430	11.58	–	
DD81-29 (1100/96)	1.51 ± 0.06	0.04	19.5	0.05	1900 ± 240	8.84	–	
DD85-17 (U)	1.57 ± 0.07	0.04	24.1	0.05	1970 ± 290	9.16	–	
DD85-17 (850/48)	1.67 ± 0.10	0.04	29.3	0.06	2100 ± 410	9.77	–	
DD85-17 (1100/96)	1.62 ± 0.07	0.04	23.7	0.05	2040 ± 300	9.49	–	
WRS-1348 (U)	1.61 ± 0.05	0.04	17.1	0.05	2030 ± 190	9.44	0.06–0.09	(3)
Fish Canyon Tuff (U)	1.65 ± 0.08	0.04	24.0	0.06	2080 ± 330	9.67	0.01–0.05	(4)
10 shot analyses								
91500 (U)	0.56 ± 0.02	0.01	15.0	0.02	704 ± 23	3.27	0.04–0.05	(1)
Plešovice (U)	0.62 ± 0.01	0.02	8.6	0.02	779 ± 17	3.60	0.08–0.57	(2)
WRS-1348 (U)	0.70 ± 0.02	0.02	15.5	0.02	880 ± 35	4.09	0.02–0.04	(3)
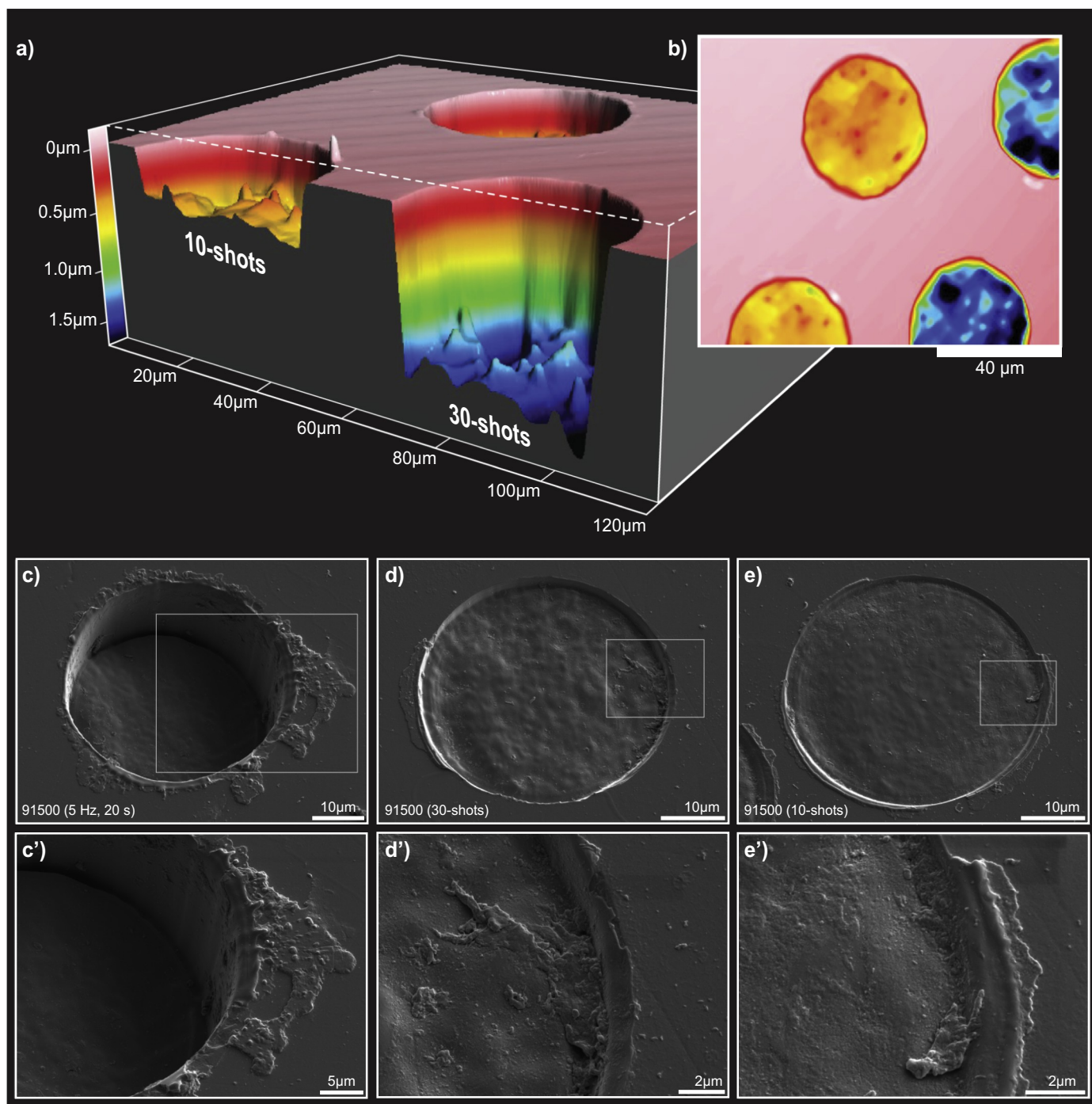
Fig. 6. (a) A 3-dimensional rendering of the crater morphologies resulting from 30 and 10 shot analyses of Plešovice (U) measured by WLI. It should be noted that the vertical scaling of this graphic is exaggerated. (b) A plan view of the same Plešovice (U) sample surface. This view evidences inhomogeneous sampling at the crater floor. (c-c') Secondary electron SEM images of a static high frequency ablation (5 Hz, 20 s) conducted on 91500 (U), where all other analytical parameters are maintained as employed for multi-shot analysis. Evidence of significant welding and analyte re-deposition is present. The white box in (c) represents the magnified view of the re-deposited material presented in (c'). (d-d') Secondary electron SEM images of a crater generated by 30 consecutive shots on the same fragment of 91500. The crater aspect ratio, as well as the degree of melt generation and re-deposition are significantly reduced relative to that observed in (c) and (c'). (e-e') Secondary electron SEM images of a crater generated by 10 consecutive shots on the same fragment of 91500. The crater aspect ratio, as well as the degree of melt generation and re-deposition are again comparatively reduced to that observed in the high frequency static ablation (c-c').

Declaration of competing interest

The authors declare that they have no known competing financial interests or personal relationships that could have appeared to influence the work reported in this paper.

Acknowledgments

DD85-17. David Chew is thanked for providing zircon sample WRS-1348 and for providing helpful discussion on the manuscript. Leona O'Connor is thanked for her assistance with the WLI instrument. Paul Guyett is thanked for his assistance in collecting the SEM images. The anonymous reviewers are also thanked for their constructive comments, which helped improve the manuscript.

Appendix A. Supplementary data

An annotated copy of the NICE script v.2 has been included as a python formatted text file in the online version of this article. Working copies of the NICE scripts described herein can be acquired from the associated online data repository or by contacting Nu.attomservice@ametek.com directly. Supplementary data to this article can be found online at doi: https://doi.org/10.1016/j.chemgeo.2020.119568.

References

Allen, C.M., Campbell, I.H., 2012. Identification and elimination of a matrix-induced systematic error in LA-ICP–MS ^{206}Pb/^{238}U dating of zircon. Chem. Geol. 332-333, 157–165. https://doi.org/10.1016/j.chemgeo.2012.09.038.

Bachmann, O., Oberli, F., Dungan, M.A., Meier, M., Mundil, R., Fischer, H., 2007. ^{40}Ar/^{39}Ar and U–Pb dating of the fish Canyon magmatic system, San Juan Volcanic field, Colorado: evidence for an extended crystallization history. Chem. Geol. 236, 134–166. https://doi.org/10.1016/j.chemgeo.2006.09.005.

Bleiner, D., Günther, D., 2001. Theoretical description and experimental observation of aerosol transport processes in laser ablation inductively coupled plasma mass spectrometry. J. Anal. At. Spectrom. 16 (5), 449–456. https://doi.org/10.1039/B009729m.

Chew, D., Drost, K., Petrus, J., 2018. Ultrafast, > 50 Hz LA-ICP-MS spot analysis applied to U–Pb dating of zircon and other U-bearing minerals. Geostand. Geoanal. Res. 43, 39–60. https://doi.org/10.1111/ggr.12257.

Cottle, J.M., Horstwood, M.S.A., Parrish, R.R., 2009. A new approach to single shot laser ablation analysis and its application to in situ Pb/U geochronology. J. Anal. At. Spectrom. 24, 1355–1363. https://doi.org/10.1039/b821899d.

Cottle, J.M., Kylander-Clark, A.R., Vrijmoed, J.C., 2012. U–Th/Pb geochronology of detrital zircon and monazite by single shot laser ablation inductively coupled plasma mass spectrometry (SS-LA-ICPMS). Chem. Geol. 332-333, 136–147. https://doi.org/10.1016/j.chemgeo.2012.09.035.

Crowley, Q.G., Heron, K., Riggs, N., Kamber, B.S., Chew, D., McConnell, B., Benn, K., 2014. Chemical abrasion applied to LA-ICP-MS U–Pb zircon geochronology. Minerals 4, 503–518. https://doi.org/10.3390/min4020503.

Davis, D.W., Edwards, G.R., 1986. Crustal evolution of Archean rocks in the Kakagi Lake area, Wabigoon subprovince, Ontario, as interpreted from high-precision U-Pb geochronology. Can. J. Earth Sci. 23, 182–192. https://doi.org/10.1139/e86-021.

Deer, W.A., Howie, R.A., Zussman, J., 1992. An Introduction to the Rock-Forming Minerals, 2nd ed. Longman, London, UK, pp. 1992.

Eggins, S.M., Kinsley, L.P.J., Shelley, J.M.G., 1998. Deposition and element fractionation processes during atmospheric pressure laser sampling for analysis by ICP-MS. Appl. Surf. Sci. 127-129, 278–286. https://doi.org/10.1016/S0169-4332(97)00643-0.

Fernández, Beatriz, Claverie, Fanny, Pécheyran, Christophe, Donard, Olivier, 2007. Direct analysis of solid samples by fs-LA-ICP-MS. Trends Anal. Chem. 26 (10), 951–966. https://doi.org/10.1016/j.trac.2007.08.008. https://doi.org/10.1016/j.trac.2007.08.008.

Fisher, C.F., Longerich, H.P., Jackson, S.E., Hanchar, J.M., 2010. Data acquisition and calculation of U–Pb isotopic analyses using laser ablation (single collector) inductively coupled plasma mass spectrometry. J. Anal. At. Spectrom. 25 (12), 1905–1920. https://doi.org/10.1039/C004955G.

Fryer, B.J., Jackson, S.E., Longerich, H.P., 1995. Design, operation and role of the Laser-Ablation Microprobe Coupled with an Inductively-Coupled Plasma Mass Spectrometer (LAM-ICP-MS) in the Earth-Sciences. Can. Mineral. 33 (2), 303–312. https://doi.org/10.1016/0009-2541(93)90058-Q.

Guillong, M., Günther, D., 2002. Effect of particle size distribution on ICP-induced elemental fractionation in laser ablation-inductively coupled plasma-mass spectrometry. J. Anal. At. Spectrom. 17 (8), 831–837. https://doi.org/10.1039/B202988J.

Günther, D., Heinrich, C.A., 1999. Enhanced sensitivity in laser ablation-ICP mass spectrometry using helium-argon mixtures as aerosol carrier. J. Anal. At. Spectrom. 14, 1363–1368. https://doi.org/10.1039/A901648A.

Hirata, T., Nesbitt, R.W., 1995. U-Pb isotope geochronology and zircon: evaluation of the laser probe-inductively coupled plasma mass spectrometry technique. Geochim. Cosmochim. Acta 59, 2491–2500. https://doi.org/10.1016/0016-7037(95)00144-1.

Horn, I., Günther, D., 2003. The influence of ablation carrier gasses Ar, He and Ne on the particle size distribution and transport efficiencies of laser ablation-induced aerosols: implications for LA–ICP–MS. Appl. Surf. Sci. 207, 144–157. https://doi.org/10.1016/S0169-4332(02)01324-7.

Horn, I., Rudnick, R.L., McDonagh, W.F., 2000. Precise elemental and isotope ratio determination by simultaneous solution nebulization and laser ablation-ICP-MS: application to U–Pb geochronology. Chem. Geol. 164 (3–4), 281–301. https://doi.org/10.1016/S0009-2541(99)00168-0.

Horstwood, M.S.A., 2008. Data reduction strategies, uncertainty assessment and

resolution of LA-(MC-)ICP-MS isotope data. In: Sylvester, P. (Ed.), Laser Ablation ICP-MS in the Earth Sciences: Current Practices and Outstanding Issues. Mineral. Assoc. Canpp. 283–303. (Short course, 40, 40). http://nora.nerc.ac.uk/id/eprint/5731/.

Horstwood, M.S.A., Košler, J., Gehrels, G., Jackson, S.E., McLean, N.M., Paton, C., Pearson, N.J., Sircombe, K.N., Sylvester, P., Vermeesch, P., Bowring, J.F., Condon, D.J., Schoene, B., 2016. Community-derived standards for LA-ICP-MS U-(Th-)Pb geochronology – uncertainty propagation, age interpretation and data reporting. Geostand. Geoanal. Res. 40, 311–332. https://doi.org/10.1111/j.1751-908X.2016.00379.x.

Jackson, S.E., Pearson, N.J., Griffin, W.L., Belousova, E., 2004. The application of laser ablation-inductively coupled plasma-mass spectrometry to in situ U–Pb zircon geochronology. Chem. Geol. 211 (1–2), 47–69. https://doi.org/10.1016/j.chemgeo.2004.06.017.

Jaffey, A.H., Flynn, K.F., Glendenin, L.E., Bentley, W.C., Essling, A.M., 1971. Precision measurement of half-lives and specific activities of ^{235}U and ^{238}U. Phys. Rev. Series C4, 1889–1905. https://doi.org/10.1103/PhysRevC.4.1889.

Koch, J., Feldmann, I., Jakubowski, N., Niemax, K., 2002. Elemental composition of laser ablation aerosol particles deposited in the transport tube to an ICP. Spectrochim. Acta Part B. 57, 975–985. https://doi.org/10.1016/S0584-8547(02)00021-6.

Kooijman, E., Berndt, J., Mezger, K., 2012. U-Pb dating of zircon by laser ablation ICP-MS: recent improvements and new insights. Eur. J. Mineral. 24, 5–21. https://doi.org/10.1127/0935-1221/2012/0024-2170.

Košler, J., Wiedenbeck, M., Wirth, R., Hovorka, J., Sylvester, P., Míková, J., 2005. Chemical and phase composition of particles produced by laser ablation of silicate glass and zircon – Implication for elemental fractionation during ICP-MS analysis. J. Anal. At. Spectrom. 20 (5), 402–409. https://doi.org/10.1039/b416269b.

Košler, J., Sláma, J., Belousova, E., Corfu, F., Gehrels, G.E., Gerdes, A., Horstwood, M.S.A., Sircombe, K.N., Sylvester, P., Tiepolo, M., Whitehouse, M.J., Woodhead, J.D., 2013. U-Pb detrital zircon analysis - results of an inter-laboratory comparison. Geostand. Geoanal. Res. 37, 243–259. https://doi.org/10.1111/j.1751-908X.2013.00245.x.

Kroslakova, I., Günther, D., 2007. Elemental fractionation in laser ablation- inductively coupled plasma-mass spectrometry: evidence for mass load induced matrix effects in the ICP during ablation of a silicate glass. J. Anal. At. Spectrom. 22, 51–62. https://doi.org/10.1039/B606522H.

Kuhn, H.R., Guillong, M., Günther, D., 2004. Size-related vaporisation and ionisation of laser-induced glass particles in the inductively coupled plasma. Anal. Bioanal. Chem. 378 (4), 1069–1074. https://doi.org/10.1007/s00216-003-2346-7.

Kuhn, B.K., Birbaum, K., Luo, Y., Günther, D., 2009. Fundamental studies on the ablation behaviour of Pb/U in NIST 610 and zircon 91500 using laser ablation inductively coupled plasma mass spectrometry with respect to geochronology. J. Anal. At. Spectrom. 25, 21–25. https://doi.org/10.1039/B917261K.

Liu, H., Borisov, O., Mao, X., Shuttleworth, S., Russo, R., 2000. Pb/U Fractionation during Nd:YAG 213 nm and 266 nm Laser Ablation Sampling with Inductively coupled Plasma Mass Spectrometry. Appl. Spectrosc. 54 (10), 1435–1442.

Longerich, H.P., Jackson, S.E., Günther, D., 1996. Inter-laboratory note. Laser ablation inductively coupled plasma mass spectrometric transient signal data acquisition and analyte concentration calculation. J. Anal. At. Spectrom. 11 (9), 899–904. https://doi.org/10.1039/JA9961100899.

Mank, A.J.G., Mason, P.R.D., 1999. A critical assessment of laser ablation ICP-MS as an analytical tool for depth analysis in silica-based glass samples. J. Anal. At. Spectrom. 14 (8), 1143–1153. https://doi.org/10.1039/A903304A.

Mank, A.J.G., Mason, P.R.D., 2001. Depth-resolved analysis in multi-layered glass and metal materials using laser ablation inductively coupled plasma mass spectrometry (LA-ICP-MS). J. Anal. At. Spectrom. 16, 1381–1388. https://doi.org/10.1039/B106932B.

Marillo-Sialer, E., Woodhead, J.D., Hergt, J., Grieg, A., Guillong, M., Gleadow, A., Evans, N., Paton, C., 2014. The zircon "matrix effect": evidence for an ablation rate control on the accuracy of U–Pb age determinations by LA-ICP-MS. J. Anal. At. Spectrom. 29 (6), 981. https://doi.org/10.1039/c4ja00008k.

Marillo-Sialer, E., Woodhead, J.D., Hanchar, J.M., Reddy, S.M., Greig, A., Hergt, J., Kohn, B., 2016. An investigation of the laser-induced zircon `matrix effect. Chem. Geol. 438, 11–24. https://doi.org/10.1016/j.chemgeo.2016.05.014.

Mattinson, J., 2005. Zircon U–Pb chemical abrasion (bCA-TIMSQ) method: combined annealing and multi-step partial dissolution analysis for improved precision and accuracy of zircon ages. Chem. Geol. 220, 47–66. https://doi.org/10.1016/j.chemgeo.2005.03.011.

Nasdala, L., Kronz, A., Hanchar, J.M., Tichomirowa, M., Davis, D.W., Hofmeister, W., 2006. Effects of natural radiation damage on back-scattered images of single crystals of minerals. Am. Mineral. 91, 1739–1746. https://doi.org/10.2138/am.2006.2241.

Pointon, M.A., Cliff, R.A., Chew, D., 2012. The provenance of Western Irish Namurian Basin sedimentary strata inferred using detrital zircon U–Pb LA-ICP-MS geochronology. Geol. J. 47, 77–98. https://doi.org/10.1002/gj.1335.

Russo, R.E., Mao, X.L., Borisov, O.V., Liu, H., 2000. Influence of wavelength on fractionation in laser ablation ICP-MS. J. Anal. At. Spectrom. 15, 1115–1120. https://doi.org/10.1039/B004243I.

Shaheen, M.E., Gagnon, J.E., Fryer, B.J., 2012. Femtosecond (fs) lasers coupled with modern ICP-MS instruments provide new and improved potential for in situ elemental and isotopic analyses in the geosciences. Chem. Geol. 330-331, 260–273. https://doi.org/10.1016/j.chemgeo.2012.09.016.

Simonetti, A., Heaman, L.M., Hartlaub, R.P., Creaser, R.A., MacHattie, T.G., Böhm, C., 2005. U–Pb zircon dating by laser ablation-MC-ICP-MS using a new multiple ion counting Faraday collector array. J. Anal. At. Spectrom. 20, 677–686. https://doi.org/10.1039/b504465k.

Sláma, J., Košler, J., Condon, D.J., Crowley, J.L., Gerdes, A., Hanchar, J.M., Horstwood, M.S.A., Morris, G.A., Nasdala, L., Norberg, N., Schaltegger, U., Schoene, B., Tubrett,

M.N., Whitehouse, M.J., 2008. Plešovice zircon—a new natural reference material for U-Pb and Hf isotopic microanalysis. Chem. Geol. 249, 1–35. https://doi.org/10.1016/j.chemgeo.2007.11.005.

Spencer, C.J., Kirkland, C.L., Taylor, R.J.M., 2016. Strategies towards statistically robust interpretations of in situ U-Pb zircon geochronology. Geosci. Front. 7, 581–589. https://doi.org/10.1016/j.gsf.2015.11.006.

Steiger, R.H., Jäger, E., 1977. Subcommission on geochronology: Convention on the use of decay constants in geo- and cosmochronology. Earth Planet. Sci. Lett. 36, 359–362. https://doi.org/10.1016/0012-821X(77)90060-7.

Tomlinson, K.Y., Davis, D.W., Stone, D., Hart, T.R., 2003. U–Pb Age and Nd Isotopic Evidence for Archean Terrane Development and Crustal Recycling in the South-Central Wabigoon Subprovince, Canada. 144. pp. 684–702. https://doi.org/10.1007/s00410-002-0423-0.

Vermeesch, P., 2018. IsoplotR: a free and open toolbox for geochronology. Geosci. Front. 9, 1479–1493. https://doi.org/10.1016/j.gsf.2018.04.001.

Wiedenbeck, M., Allé, P., Corfu, F., Griffin, W.L., Meier, M., Oberli, F., von Quadt, A., Roddick, J.C., Spiegel, W., 1995. Three natural zircon standards for U-Th-Pb, Lu-Hf, trace element and REE analyses. Geostand. Newslett. 19, 1–23. https://doi.org/10.1111/j.1751-908X.1995.tb00147.x.

Woodhead, J.D., Hergt, J.M., 2001. Strontium, neodymium and lead isotope analyses of NIST glass certified reference materials: SRM 610, 612, 614. Geostand. Newslett. 25 (2–3), 261–266. https://doi.org/10.1111/j.1751-908X.2001.tb00601.x.